ACS APPLIED MATERIALS & INTERFACES

Research Article

Cite This: ACS Appl. Mater. Interfaces 2018, 10, 22834−22840

www.acsami.org

Conformal Electroless Nickel Plating on Silicon Wafers, Convex and Concave Pyramids, and Ultralong Nanowires

Thomas Mark Gill,[†] Jiheng Zhao,[†] Erwin J. W. Berenschot,[‡] Niels Tas,[‡] and Xiaolin Zheng*[,†]

[†]Department of Mechanical Engineering, Stanford University, Stanford, California 94305, United States

[‡]MESA Research Institute for Nanotechnology, University of Twente, P.O. Box 217, 7500 AE Enschede, Netherlands

Supporting Information

ABSTRACT: Nickel (Ni) plating has garnered great commercial interest, as it provides excellent hardness, corrosion resistance, and electrical conductivity. Though Ni plating on conducting substrates is commonly employed via electrodeposition, plating on semiconductors and insulators often necessitates electroless approaches. Corresponding plating theory for deposition on planar substrates was developed as early as 1946, but for substrates with micro- and nanoscale features, very little is known of the relationships between plating conditions, Ni deposition quality, and substrate morphology. Herein, we describe the general theory and mechanisms of electroless Ni deposition on semiconducting silicon (Si) substrates, detailing plating bath failures and establishing relationships between critical plating bath parameters and the deposited Ni film quality. Through this theory, we develop two different plating recipes: galvanic displacement (GD) and autocatalytic deposition (ACD). Neither recipe requires pretreatment of the Si substrate, and both methods are capable of depositing uniform Ni films on planar Si substrates and convex Si pyramids. In comparison, ACD has better tunability than GD, and it provides a more conformal Ni coating on complex and high-aspect-ratio Si structures, such as inverse fractal Si pyramids and ultralong Si nanowires. Our methodology and theoretical analyses can be leveraged to develop electroless plating processes for other metals and metal alloys and to generally provide direction for the adaptation of electroless deposition to modern applications.

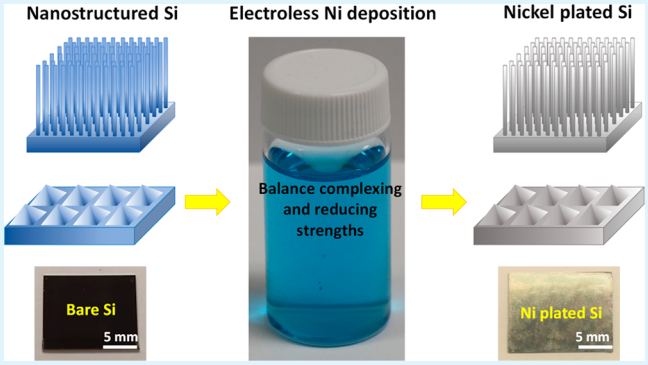

KEYWORDS: *electroless plating, electroless nickel plating, nickel plating on Si, Si nanowires, and Si pyramids*

1. INTRODUCTION

Metal plating, because of its ability to create desirable thermal, electrical, and physical properties, has gained prominence in a variety of manufacturing processes.[1−3] Plating using wet electrochemical methods, such as electroplating and electroless deposition, is particularly attractive owing to its simplicity and scalability.[4,5] Holistically, electroless plating offers several distinct advantages over electrodeposition: it can coat nonconductive and semiconducting substrates, does not require external electrical energy, and can produce uniform deposits on acute morphologies where electrodeposition suffers from conformal buildup.[6,7] Among metals, nickel (Ni) has been broadly applied to metal surfaces for wear resistance, hardness enhancement, and corrosion protection, resulting in the development of several reliable plating recipes on conductive materials.[8−11] In particular, electroless Ni plating on semiconductors, such as silicon (Si), has garnered recent interest due to its potential applications spanning from microelectronics and solar cells to chemical catalysis.[12,13]

The general theory for nickel electroless plating was largely established from 1940 to 1975,[14−17] including explanation of the mechanisms for nickel deposition on planar substrates. Studies published in the past 15 years, however, are largely empirical, detailing only successful electroless methods for the application of interest.[18−22] With the advancement of nanotechnology, contemporary research often also involves plating on substrates with complex small-scale morphologies.[20,21,23] These trends have left a void in the electroless deposition literature, as very little work has been done to elucidate the connections between pertinent plating bath parameters, substrate morphology, and deposition quality. Accordingly, the adaptation of electroless methods for modern substrates, especially those with micro- and nanoscale features, is largely unguided and often leads to inefficient trial and error efforts.

Herein, we investigate the mechanism of two popular electroless Ni plating methods on Si—galvanic displacement (GD) and autocatalytic deposition (ACD)—and develop simplified recipes for Ni deposition on complex Si substrates. Neither method uses HF pretreatment of Si to remove native oxides, nor any precious metal nucleation initiators (e.g., Pd), both of which are used in most Ni on Si studies.[12,24−27] These procedural simplifications allow for elucidation of the relation-

Received: April 13, 2018
Accepted: June 8, 2018
Published: June 8, 2018

DOI: 10.1021/acsami.8b06002
ACS Appl. Mater. Interfaces 2018, 10, 22834−22840

ship between bath parameters, deposition mechanisms, morphology, and deposition quality. Thermodynamically, both methods function because the reduction potential of the nickel ions (Ni^{2+}) is more positive than that of the reducing agents. For GD, the reducing agent is the Si substrate itself, offering simple implementation. For ACD, a separate reducing agent (e.g., BH_4^-) is used together with a complexing agent, which controls the concentration of Ni^{2+} and allows for greater tunability. We have experimentally identified the correlation between the reduction potential of the reducing agent and the strength of the complexing agent in ACD baths. This correlation enables the substitution of suitable reducing agents for specific applications in place of more conventional agents used for electroless Ni on Si (e.g., sodium hypophosphite). For both GD and ACD, conformal Ni plating is realized on planar Si and convex Si pyramids. Because of its deposition mechanism and high tunability, ACD provides more conformality than does GD for complex and high-aspect-ratio Si structures, such as inverse fractal Si pyramids and ultralong Si nanowires (>350 μm). These experimental results, coupled with the theory developed in this study, will help guide the development of electroless plating of other metals and metal alloys on various silicon morphologies and will enable the adaptation of electroless metal plating for new applications.

As a side note, the nomenclature used for various deposition mechanisms in the original electroless plating literature is somewhat convoluted. Because our mechanistic descriptions match theirs fairly well, we follow the usages developed by Djokić and Cavallotti, who identify ACD and GD as two subcategories of electroless deposition.[28]

2. EXPERIMENTAL METHODS

Phosphorus doped n-type silicon (n-Si) wafers with native oxides (1−4 Ω cm, (100), WRS Materials) were cut into approximately 1.5 cm by 2.0 cm pieces. The pieces were sequentially cleaned under sonication in acetone, isopropyl alcohol (IPA), and water and finally dried under air to remove any contaminants from the Si surface. Convex Si pyramid substrates were prepared by anisotropically etching n-Si wafers for 2 h using 1 M KOH at 80 °C. Concave nanoscale fractal Si pyramids were prepared by the previously reported corner lithography method combined with anisotropic etching.[29] Ultralong Si nanowires were prepared by electro-assisted, metal-assisted chemical etching, a method previously developed by our group.[30]

All reagents in this work were purchased from Sigma-Aldrich (unless otherwise noted) and used as received. Three solutions were prepared for the electroless Ni plating baths. First, nickel precursor solution was prepared by combining 0.05 M nickel(II) sulfate hexahydrate ($NiSO_4 \cdot 6H_2O$, 99%) as a nickel ion source and 0.05 M sodium phosphate monobasic monohydrate ($NaH_2PO_4 \cdot H_2O$, ≥98%) as a buffer. Second, a solution of 0.1 M sodium borohydride ($NaBH_4$, 99%) was prepared as a reducing agent. Finally, a solution of 0.1 M sodium citrate tribasic dihydrate ($Na_3C_6H_5O_7 \cdot 2H_2O$, ≥99%) was prepared as a complexing agent. Each solution was made with DI water and sonicated thoroughly to ensure homogeneous mixing.

For the GD method, the plating bath contains only the nickel/buffer solution described above. The pH of the bath solution was tuned to 9.0 ± 0.1 using ammonium hydroxide (NH_4OH, 28−30%, Fisher Chemical). Si substrates were immersed in 15 mL of the bath solution, and the Si substrate-containing vials were then submerged in an oil bath at 90 °C for 20 min. Finally, the Si substrates were rinsed and sonicated in IPA and subsequently DI water, followed by drying under air prior to analysis.

For the ACD method, the bath contains the nickel, reducing, and complexing solutions in volumetric ratios of 15:1:4, respectively, thereby maintaining the same amount of nickel salt as in the GD bath. The pH of the bath solution was tuned to 10.1 ± 0.1 using ammonium hydroxide (NH_4OH, 28−30%, Fisher Chemical). Si substrates were immersed in 20 mL of the bath solution, and the Si substrate-containing vials were then submerged in an oil bath at 90 °C for 1 h. Finally, the Si substrates were rinsed and sonicated in IPA and subsequently DI water, followed by drying under air prior to analysis. In the case of electroless Ni plating on Si nanowires, a few milliliters of ethanol was added to the bath solution to reduce the surface tension of the liquid in the solution, thereby allowing it to percolate into the spaces between the high-aspect-ratio nanowires.

The resulting Ni structure and deposition were studied using a scanning electron microscope (SEM) with a field emission gun (FEI XL30, Sirion). Composition of the metals deposited on the substrates was determined using an X-ray photoelectron spectroscope (XPS) with a monochromatized Al Kα source (PHI Versaprobe I, Physical Electronics Inc.). Finally, crystallography and compositional confirmation were obtained using an X-ray diffractometer (XRD) (MRD X'Pert, PANalytical).

3. DISCUSSION OF MECHANISM OF ELECTROLESS Ni PLATING

3.1. Thermodynamic Analysis. Figure 1a shows the reaction mechanism of GD between SiO_2/Si and Ni^{2+}/Ni.

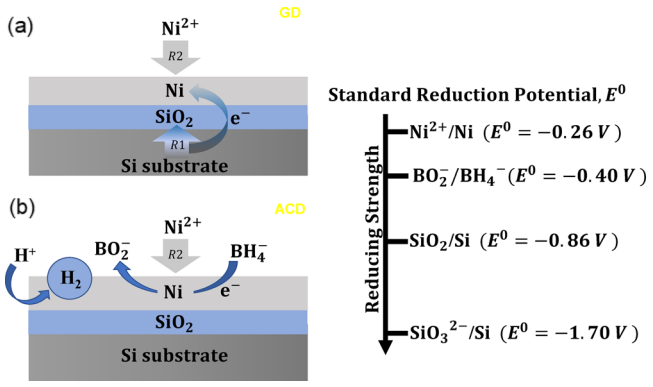

Figure 1. Schematic of mechanism for nickel deposition via GD (a) and ACD (b) and standard reduction potentials of constituents of interest in electroless nickel deposition on silicon. Reaction 1 (R1) above: $Si_{(s)} + 4OH^- \leftrightarrow SiO_2 + 2H_2O + 4e^-$. Reaction 2 (R2) above: $2Ni^{2+} + 4e^- \leftrightarrow 2Ni_{(s)}$.

The standard reduction potential of SiO_2/Si (−0.86 V) is far more negative than that of Ni^{2+}/Ni (−0.26 V), indicating that thermodynamics favor the reduction of Ni^{2+} by Si. In alkaline conditions, the anodic and cathodic half-reactions are expressed as follows:

$$\text{anode:} \quad Si_{(s)} + 4OH^- \leftrightarrow SiO_2 + 2H_2O + 4e^- \qquad (R1)$$

$$\text{cathode:} \quad 2Ni^{2+} + 4e^- \leftrightarrow 2Ni_{(s)} \qquad (R2)$$

In this manner, the oxidation of the Si substrate produces electrons which serve to reduce Ni^{2+} ions present in the growth precursor, leading to Ni deposition on Si.

The ACD bath is similar to more traditional electroless nickel baths in that it contains a source of nickel ions, a complexing agent, and a reducing agent (sodium borohydride, $NaBH_4$).[31,32] Figure 1 shows that the standard reduction potential of BO_2^-/BH_4^- (−0.40 V) is more negative than that of Ni^{2+}/Ni (−0.26 V), indicating that, thermodynamically, $NaBH_4$ can reduce Ni^{2+} in the bath solution.

For both GD and ACD, the presence of a thin native oxide layer (SiO_2, 2−5 nm) prior to immersion in plating solution is not problematic, as SiO_2 is further oxidized to SiO_3^{2-} in strong

DOI: 10.1021/acsami.8b06002
ACS Appl. Mater. Interfaces 2018, 10, 22834−22840

alkaline environments ($2OH^- + SiO_2 \rightarrow SiO_3^{2-} + H_2O$).[33,34] Accordingly, this demonstrates the theoretical efficacy of nickel deposition via GD and ACD without pretreating the silicon substrate.

3.2. GD and ACD Ni Plating Solution Compositions and Their Functions. Since the GD bath solution is alkaline, Ni^{2+} cations form nickel hydroxide ($Ni(OH)_2$),[35] resulting in a turbid green solution (see GD bath in Figure 2b). However,

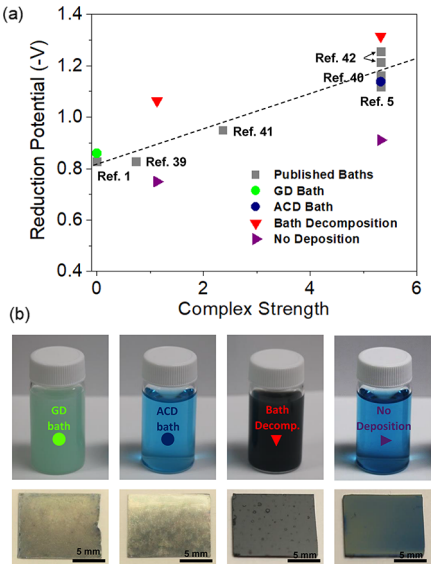

Figure 2. Plot of reduction potential of reducing agent vs complex strength of nickel complex for several investigated baths and previously reported electroless nickel baths on silicon (a). Specific conditions for each bath are given in Table S1. The fitted dashed line suggests theoretically viable plating baths for electroless nickel on silicon. Characteristic solution appearance for plotted baths and their corresponding deposition results on n-Si (b).

$Ni(OH)_2$ has high solubility among metal hydroxides (0.13 g/L in water), allowing for the presence of a substantial concentration of Ni^{2+} ions in the solution.[35−37] Additionally, the standard reduction potential of SiO_2/Si (−0.86 V) is more negative than that of $Ni(OH)_2$ /Ni (−0.721 V), meaning that galvanic displacement is still energetically feasible, even if most of the nickel ion source remains in the hydroxide precipitate. Accordingly, the GD bath needs only a nickel salt and a pH buffer.

Contrastingly, the ACD bath contains a complexing agent, sodium citrate, which supplies citrate ions to bond to the Ni^{2+} cations as ligands, forming a metal complex. This inhibits the formation of the relatively inert $Ni(OH)_2$, leading to a transparent blue solution (see ACD bath in Figure 2b). The metal complex also controls the concentration of free Ni^{2+} cations in the solution, thereby influencing the plating rate.[31,32] Correspondingly, the reducing agent needs to have a low enough reduction potential (i.e., is strong enough) to reduce the nickel ions in the solution. As a result, most reported electroless Ni plating solutions have used sodium hypophosphite as the reducing agent due to its very negative reduction potential.[31] However, hypophosphite salts are classified by the United States Drug Enforcement Administration (USDEA) as a List I substance, which inhibits their use in research and manufacturing.[38] Accordingly, we have developed the following theory to substitute another known reducing agent, $NaBH_4$, as a less restrictive alternative for Ni plating on silicon in the method of the ACD bath.

3.3. Balance between Reduction Potential and Complexing Strength for Electroless Ni Plating. Successful electroless Ni plating requires a balance between the reduction potential of the reducing agent and the complexing strength, as illustrated in Figure 2, which summarizes plating solutions in this study and others from previous reports.[1,5,39−42] Its ordinate axis (reduction potential) indicates the reduction strength of a reducing agent,[43] as determined by the modified Nernst equation:

$$E = E^0 - 2.303\frac{RT}{nF}\mathrm{pH}$$

Here, n is the stoichiometric number of moles of electrons transferred, R is the universal gas constant, T is the absolute temperature of the plating bath, and F is Faraday's constant. For example, the oxidation of the borohydride anion ($BH_4^- + 8OH^- \leftrightarrow BO_2^- + 6H_2O + 8e^-$, $E^0 = -0.40$ V) yields 1 mol of electrons per mole of hydroxide anion present ($n = 1$).[43] The conditions established in the ACD bath ($T = 363$ K, pH = 10.1) thus yield a reduction potential of $E = -1.13$ V. In accordance with the Nernst equation, the pH, temperature, and component concentrations in ACD baths all influence the strength of the reducing agent.[28] Through this method, the reducing strengths of several nickel plating baths for deposition on silicon reported in the literature[1,5,39−42] are calculated (Table S1, Supporting Information). The abscissa in Figure 2 (complex strength) corresponds to the equilibrium constant K for the conversion between the Ni complex and the Ni^{2+} ions, taken from a NIST database.[44] Higher complex strength indicates greater nickel complex stability, requiring a stronger reduction potential (i.e., higher pH or temperature) to induce Ni plating.

The dashed line in Figure 2 is a linear fit through successful Ni plating solutions, including our GD (green dot) and ACD (blue dot) solutions, and baths reported by others for electroless Ni on Si.[1,5,39−42] The strong linear correlation indicates that the complexing and reducing strengths need to match for high quality Ni plating. For our GD and ACD baths, the deposited Ni film appears uniform and gives a metal-like finish on Si (Figure 2b). When the Ni plating solution conditions deviate from this linear relation, plating of poor quality or no plating results. For example, when the reduction potential is much higher than this linear relation (red triangles, Figure 2), bulk reduction of Ni ions occurs in the solution, forming black precipitation (see "Bath Decomposition" in Figure 2b).[32,45,46] Ni is also deposited on Si in this case but with very poor quality and adhesion, as shown by the grayish color in Figure 2b. On the contrary, when the complex strength is too high (purple triangles, Figure 2), there is minimal reduction of Ni ions, leading to little deposition on Si (Figure 2b). Hence, this linear fitting provides important guidance for tuning the plating bath solution. For our ACD solution, the complex strength of sodium citrate is ∼5.32, and our linear fitting gives a desired reducing potential of $E \sim -1.13$ V. Using the Nernst equation, the corresponding pH at temperatures near 90 °C is calculated to be ∼10.1, giving us a theoretical starting point for our experiments.

Two important notes on electroless nickel deposition should be made here. First, both GD and ACD are accompanied by the evolution of hydrogen gas bubbles on the silicon surface (Figure 1b).[31,32,47] GD evolves hydrogen in small quantities as a result of silicon being further oxidized to SiO_3^{2-} ($Si + 2OH^- + H_2O \rightarrow SiO_3^{2-} + 2H_2\uparrow$). ACD evolves additional hydrogen due in part

DOI: 10.1021/acsami.8b06002
ACS Appl. Mater. Interfaces 2018, 10, 22834−22840

to hydrogen liberation from the borohydride anion. In both cases, failure to remove these bubbles from the surface during plating may lead to pits and pinholes in the deposited nickel layer (Figure S2). The formation of pinholes can largely be prevented by leaning the silicon wafer against the wall of the deposition vial, thereby allowing the bubbles to slide up the surface of the substrate and be released. As a final note, based on the reduction potential of silicon (Figure 1a), GD may occur in parallel with the reduction by borohydride in ACD baths, but the predominant pathway is believed to be via oxidation of the reducing agent.[31,40]

4. EXPERIMENTAL RESULTS AND DISCUSSION

So far, thermodynamic analysis has established the feasibility of GD and ACD for electroless plating Ni on Si. We have also established the relationship between the reduction potential and complex strength to achieve uniform nickel deposition on (100) n-Si (Figure 2b). Here, we examine the Ni structure and composition resulting from GD and ACD. We also investigate the application of GD and ACD to various Si morphologies to compare their deposition qualities.

4.1. Material Characterization of Electroless Deposited Ni on Si. The Ni film plated by ACD has a more reflective appearance than Ni by GD (Figure 2b). SEM images show the GD-Ni has a somewhat granular texture (Figure 3a) while the

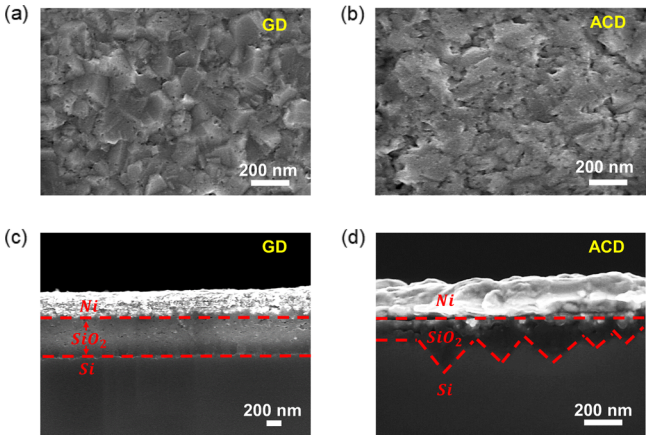

Figure 3. Top view SEM images of nickel deposited on untreated n-Si via GD (a) and ACD (b). Cross-sectional SEM images of nickel deposited on untreated n-Si via GD (c) and ACD (d).

ACD-Ni appears more continuous (Figure 3b). This is one possible reason for the apparent discrepancy in reflectivity. Both GD (20 min) and ACD (1 h) produce a uniform Ni film around 200−250 nm, suggesting that ACD is a slower deposition process (Figure 3c,d). In both cases, the cross-sectional SEM images reveal that an intermediate layer exists between Ni and n-Si (Figure 3c,d), for which the composition is determined via XPS to be SiO_2, as will be discussed later. The intermediate SiO_2 layer resulting from ACD (Figure 3d) is notably rougher than that from GD (Figure 3c), exhibiting pyramidal features. This suggests that Si and SiO_2 are etched and oxidized to SiO_3^{2-} by the ACD bath due to its higher pH and longer deposition time. Additionally, the intermediate SiO_2 layer is ∼200 nm thick on average for ACD and ∼400 nm for GD. The thinner SiO_2 layer in the ACD sample suggests that Ni^{2+} reduction via the Si substrate (i.e., the GD mechanism) plays a lesser role in the ACD bath than in the GD bath.

The chemical compositions of the as-deposited nickel and the intermediate layer were determined through XPS. Figures 4a−c show high-resolution XPS data in the Ni 2p, O 1s, and Si 2p regions, respectively, for the nickel deposited via the GD bath (red), the ACD bath (black), and samples in which the procedures of GD and ACD were carried out, followed by etching away of the deposited nickel by soaking in $FeCl_3$ for 3 min (orange and blue, respectively). This $FeCl_3$ etching step exposed the intermediate layer such that its composition could be studied. Figure 4a shows that both GD-Ni and ACD-Ni samples exhibit strong and dominant peaks at binding energies of ∼852.8 and ∼870 eV, corresponding to the $2p_{1/2}$ and $2p_{3/2}$ peaks for metallic nickel, respectively.[48] At binding energies of ∼856 and ∼873.8 eV, the GD-Ni exhibits more prominent peaks than does the ACD-Ni, denoting the presence of $Ni(OH)_2$, which is congruent with the GD bath composition.[35] The ACD-Ni shows peaks very near the $2p_{1/2}$ and $2p_{3/2}$ satellites for $Ni(OH)_2$, suggesting that it also contains $Ni(OH)_2$. The presence of $Ni(OH)_2$ in both GD-Ni and ACD-Ni samples is also confirmed by the O 1s spectrum, where both show a strong peak at ∼531.4 eV (Figure 4b), which corresponds to the energy of oxygen in $Ni(OH)_2$.[36] Both samples exhibit a very slight shoulder peak at ∼529.6 eV (Figure 4b), an energy correlated with the presence of NiO.[49] This may be the result of prolonged exposure to air prior to XPS analysis. As expected, the etched GD-Ni and ACD-Ni samples show no noticeable peaks in the Ni 2p regime, demonstrating the complete removal of nickel from the substrate surface by the $FeCl_3$. Instead, in the O 1s region, the etched samples both exhibit a singular peak very near the binding energy of oxygen in SiO_2 (∼532.8 eV), as reported by others.[50] The Si 2p spectra for both etched samples have strong peaks near 103.4 eV, a very high binding energy for silicon indicative of SiO_2 (Figure 4c).[51] The O 1s and Si 2p XPS spectra confirm that the intermediate layer is SiO_2.

The crystallinity of deposited Ni was studied using X-ray diffraction (XRD). Both GD- and ACD-Ni samples show strong peaks at $2\theta = 44.5°$ and 51.9°, matching the (111) and (200) planes of metallic nickel (ICDD PDF # 00-004-0850) (Figure 4d). The XRD spectra of the $FeCl_3$-etched GD sample (orange), $FeCl_3$-etched ACD sample (blue), and a bare, untreated n-Si substrate (green) all exhibit Si peaks at $2\theta = 47.7°$, 56.3°, and 61.7°. The notable absence of XRD peaks corresponding to $Ni(OH)_2$ indicates that the $Ni(OH)_2$ deposits either exist in small quantities or are amorphous, a well-known facet of α-phase $Ni(OH)_2$.[35] These XRD spectra also do not show peaks of SiO_2, indicating that it too is amorphous.

4.2. Deposition of Ni on Various Si Structures. We further applied both GD and ACD methods to deposit Ni on convex Si pyramids (Figure 5), fractal Si cavities (Figure 6), and ultralong Si nanowires (Figure 7) to test their capabilities. The convex Si pyramids have a characteristic width of a few micrometers. Both GD and ACD methods conformally deposit Ni over the planar surfaces and pyramids (Figure 5). The two methods show significant differences when depositing Ni on the complex fractal Si cavities (Figure 6), which contain interconnecting inverse pyramids of different sizes. The GD method mainly deposits Ni particles on the vertices of the fractal features (Figures 6a,c). This is likely caused by the fact that electrons have higher activity at the vertices than on the (111) planes, leading to concentrated Ni^{2+} reduction. Less Ni is deposited further into the depth of the cavities. By comparison, the ACD method provides relatively uniform Ni deposition throughout the entire cavity, including corners, protrusions, and

DOI: 10.1021/acsami.8b06002
ACS Appl. Mater. Interfaces 2018, 10, 22834−22840

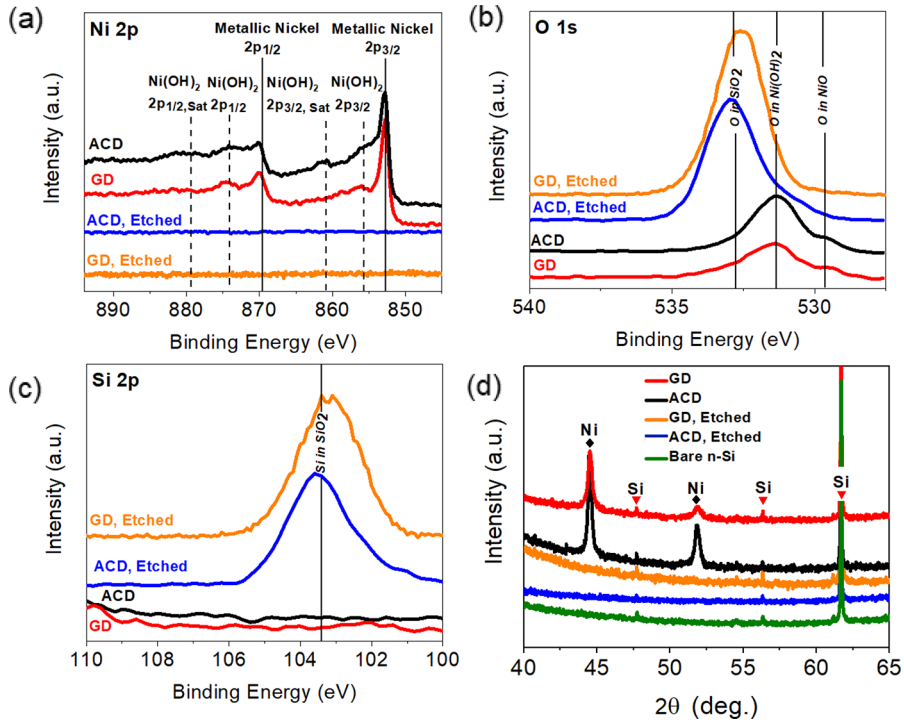

Figure 4. Material characterization of Ni deposited on n-Si. Ni 2p (a), O 1s (b), and Si 2p (c) XPS measurements of as-deposited nickel via GD (red), ACD (black), and GD and ACD samples etched with $FeCl_3$ to remove nickel layer and expose the underlying substrate (orange and blue, respectively). XRD spectra of unetched and $FeCl_3$ etched ACD and GD samples, along with bare n-Si (d).

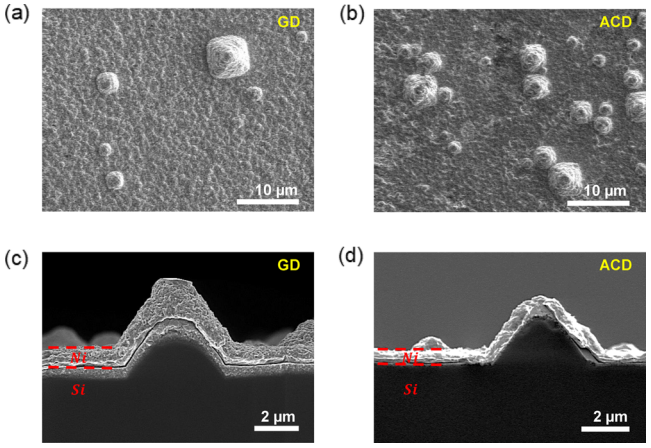

Figure 5. Top view SEM of nickel deposition on silicon pyramids via GD (a) and ACD (b) baths. Cross-sectional SEM image of nickel deposition on etched n-Si pyramids via GD (c) and ACD (d).

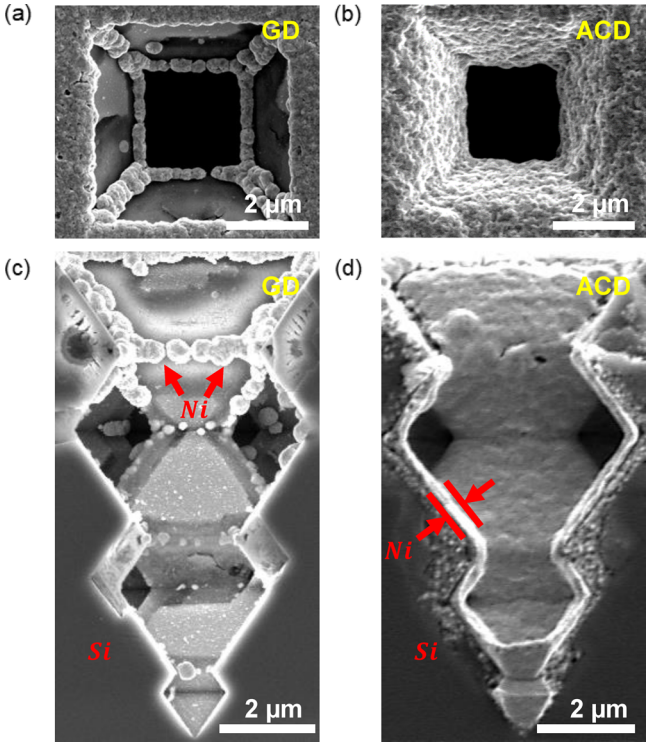

Figure 6. Top view SEM image of nickel deposition on fractal cavities of silicon via GD (a) and ACD (b). Cross-sectional SEM image of nickel deposition on fractal cavities of silicon via GD (c) and ACD (d).

even the nanoscale fractal tip (Figures 6b,d). The ACD method applied to the ultrahigh-aspect-ratio Si nanowires (length: 360 μm; diameter: 350 nm; aspect ratio: ~1000:1) (Figure 7a) conformally coated Ni from the tip to the bottom of the wires (Figures 7b–d). Small pinholes can be seen and are most dense near the base of the nanowires, which is likely due to the hydrogen bubble formation and trapping in this region in accordance with the mechanism described in Figure S2. Deposition on these Si nanowires, due to their unprecedented aspect ratio and wire density, is challenging for even the most robust plating methods.[52] The conformal coating of Ni on these Si nanowires clearly demonstrates the efficacy of the as-described ACD method for substrates with high acuity.

5. CONCLUSION

In conclusion, we have developed a general theory for electroless nickel deposition on Si. The theory identifies a linear correlation

DOI: 10.1021/acsami.8b06002
ACS Appl. Mater. Interfaces 2018, 10, 22834–22840

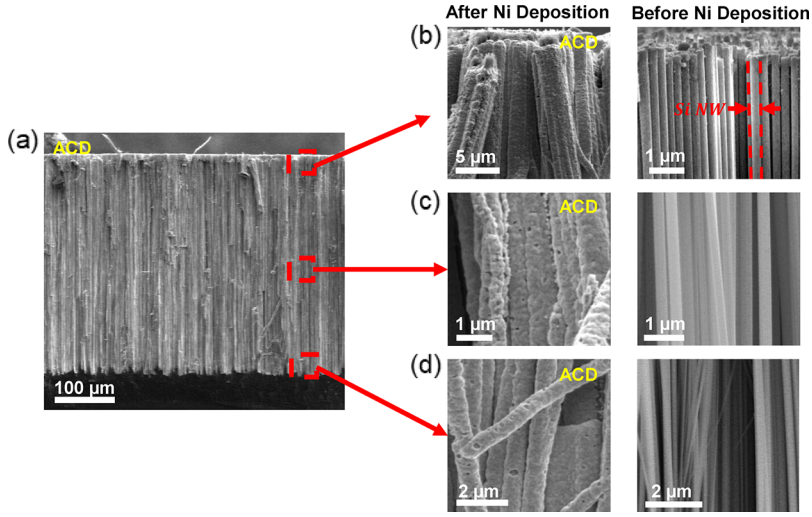

Figure 7. Cross-sectional SEM image of nickel deposition via ACD on high-aspect-ratio (~1000:1) silicon nanowires (Si NWs) (a) showing uniform coverage of the top (b), middle (c), and bottom (d) regions along the length of the wires with side-by-side comparison of silicon nanowires before nickel deposition.

between reducing potential and complex strength for high quality electroless Ni plating on Si and was leveraged to develop two electroless Ni on Si plating methods: GD and ACD. The GD bath is comprised simply of a nickel salt and a buffer and leverages the Si substrate itself to reduce Ni ions, whereas the ACD bath uses a reducing agent to reduce nickel on the silicon surface. Both GD and ACD methods are simpler than many previous electroless Ni plating methods, which has allowed us to detail the relationship between bath parameters and successful deposition without convoluting the results with the effects of pretreatment procedures. Additionally, we provide details of the failure mechanisms of the ACD bath to help streamline the electroless deposition research efforts of others. Finally, both recipes led to conformal Ni plating on planar Si and convex Si pyramids. In comparison, ACD has better tunability than GD, and it provides more conformal Ni coating on complex and high-aspect-ratio Si structures, such as inverse fractal Si pyramids and ultralong Si nanowires. The theory and methods developed in this study can be leveraged to employ similar procedures and analyses for other metals and metal alloys on insulating or semiconducting substrates, thereby leading to facile adaptation of electroless deposition for a variety of applications.

■ ASSOCIATED CONTENT

Supporting Information

The Supporting Information is available free of charge on the ACS Publications website at DOI: 10.1021/acsami.8b06002.

Plating bath conditions including pH, temperature, and constituents for references denoted in Figure 2 and for baths employed in this study; photo images of hydrogen gas evolution during ACD plating and the associated mechanism for pinhole formation (PDF)

■ AUTHOR INFORMATION

Corresponding Author

*(X.Z.) Tel (650) 736-8953; Fax (650) 723-1748; e-mail xlzheng@stanford.edu.

ORCID

Jiheng Zhao: 0000-0001-8341-9031

Niels Tas: 0000-0001-7541-4345

Xiaolin Zheng: 0000-0002-8889-7873

Author Contributions

J.Z. and T.G. performed deposition experiments, developed theory, and characterized materials. E.B. and N.T. fabricated fractal silicon cavities and provided manuscript feedback. X.Z., J.Z., and T.G. prepared the manuscript.

Funding

T.G. acknowledges funding from the Stanford University Department of Mechanical Engineering.

Notes

The authors declare no competing financial interest.

■ ACKNOWLEDGMENTS

Part of this work was performed at the Stanford Nano Shared Facilities (SNSF), supported by the National Science Foundation under Award ECCS-1542152.

■ REFERENCES

(1) Lennon, A.; Yao, Y.; Wenham, S. Evolution of metal plating for silicon solar cell metallisation. *Prog. Photovoltaics* **2013**, *21*, 1454−1468.

(2) Liu, P. S.; Liang, K. M. Review Functional materials of porous metals made by P/M, electroplating and some other techniques. *J. Mater. Sci.* **2001**, *36*, 5059−5072.

(3) Gray, J. E.; Luan, B. Protective coatings on magnesium and its alloys — a critical review. *J. Alloys Compd.* **2002**, *336*, 88−113.

(4) Niwa, D.; Homma, T.; Osaka, T. Deposition Behavior of Ni on Si(100) Surfaces in an Aqueous Alkaline Solution. *J. Electrochem. Soc.* **2005**, *152*, C54−C59.

(5) Hu, G.; Wu, H.; Yang, F. Direct electroless nickel plating on silicon surface. *Chin. Sci. Bull.* **2004**, *49*, 2363.

(6) Kundu, S.; Das, S. K.; Sahoo, P. Properties of Electroless Nickel at Elevated Temperature-a Review. *Procedia Eng.* **2014**, *97*, 1698−1706.

(7) DeMeo, D.; MacNaughton, S.; Sonkusale, S.; Vandervelde, T. In *Nanowires - Implementations and Applications*; Intech: 2011; Chapter 7, pp 141−155.

(8) Sahoo, P.; Das, S. K. Tribology of electroless nickel coatings − A review. *Mater. Eng.* **2011**, *32*, 1760−1775.

(9) Anik, M.; Körpe, E.; Şen, E. Effect of coating bath composition on the properties of electroless nickel−boron films. *Surf. Coat. Technol.* **2008**, *202*, 1718−1727.

(10) Vitry, V.; Bonin, L. Increase of boron content in electroless nickel-boron coating by modification of plating conditions. *Surf. Coat. Technol.* **2017**, *311*, 164−171.
(11) Shao, Z.; Cai, Z.; Hu, R.; Wei, S. The study of electroless nickel plating directly on magnesium alloy. *Surf. Coat. Technol.* **2014**, *249*, 42−47.
(12) Popescu, S. M.; Barlow, A. J.; Ramadan, S.; Ganti, S.; Ghosh, B.; Hedley, J. Electroless Nickel Deposition: An Alternative for Graphene Contacting. *ACS Appl. Mater. Interfaces* **2016**, *8*, 31359−31367.
(13) Zhao, J.; Gill, T. M.; Zheng, X. Enabling silicon photoanodes for efficient solar water splitting by electroless-deposited nickel. *Nano Res.* **2018**, *11*, 3499−3508.
(14) Brenner, A.; Riddell, G. Nickel Plating on Steel by Chemical Reduction. *J. Res. Natl. Bur. Stand.* **1946**, *37*, 31−35.
(15) Gorbunova, K. M.; Ivanov, M. V.; Moiseev, V. P. Electroless Deposition of Nickel-Boron Alloys Mechanism of Process, Structure, and Some Properties of Deposits. *J. Electrochem. Soc.* **1973**, *120*, 613−618.
(16) Iwasa, H.; Yokozawa, M.; Teramoto, I. Electroless Nickel Plating on Silicon. *J. Electrochem. Soc.* **1968**, *115*, 485−488.
(17) Mallory, G. O. The Electroless Nickel Plating Bath: Effect of Variables on the Process. *Plating* **1971**, *58*, 319−322.
(18) Tous, L.; van Dorp, D. H.; Russell, R.; Das, J.; Aleman, M.; Bender, H.; Meersschaut, J.; Opsomer, K.; Poortmans, J.; Mertens, R. Electroless nickel deposition and silicide formation for advanced front side metallization of industrial silicon solar cells. *Energy Procedia* **2012**, *21*, 39−46.
(19) Shong, W.-J.; Liu, C.-K.; Yang, P. Effects of electroless nickel plating on 441 stainless steel as SOFC interconnect. *Mater. Chem. Phys.* **2012**, *134*, 670−676.
(20) Weber, W. M.; Geelhaar, L.; Graham, A.; Unger, E.; Duesberg, G. S.; Liebau, M.; Pamler, W.; Cheze, C.; Riechert, H.; Lugli, P.; Kreupl, F. Silicon-Nanowire Transistors with Intruded Nickel-Silicide Contacts. *Nano Lett.* **2006**, *6* (12), 2660−2666.
(21) Kang, C.; Yuan, S.; Hong, D.; Yan, K.; et al. Superhydrophilicity/superhydrophobicity of nickel micro-arrays fabricated by electroless deposition on an etched porous aluminum template. *Chem. Eng. J.* **2012**, *203*, 1−8.
(22) Hsieh, S. H.; Hsieh, J. M.; Chen, W. J.; Chuang, C. C. Electroless Nickel Deposition for Front Side Metallization of Silicon Solar Cells. *Materials* **2017**, *10*, 942−952.
(23) Huang, T.-C.; Wu, J.-T.; Yang, S.-Y.; Huang, P.-H.; Chang, S.-H. Direct fabrication of microstructures on metal roller using stepped rotating lithography and electroless nickel plating. *Microelectron. Eng.* **2009**, *86*, 615−618.
(24) Takano, N.; Hosoda, N.; Yamada, T.; Osaka, T. Effect of oxidized silicon surface on chemical deposition of nickel on n-type silicon wafer. *Electrochim. Acta* **1999**, *44*, 3743−3749.
(25) Hsu, C.-W.; Wang, W.-Y.; Wang, K.-T.; Chen, H.-A.; Wei, T.-C. Manipulating the adhesion of electroless nickel-phosphorus film on silicon wafers by silane compound modification and rapid thermal annealing. *Sci. Rep.* **2017**, *7*, 9656−9666.
(26) Hamilton, J. F.; Logel, P. C. Catalysis of electroless nickel deposition by small palladium nuclei. *J. Catal.* **1973**, *29*, 253−263.
(27) Huang, J.; Chen, Z. Method for electroless nickel plating on the surface of CaCO 3 powders. *RSC Adv.* **2017**, *7*, 25622−25626.
(28) Djokić, S. S.; Cavallotti, P. L. In *Electrodeposition Theory and Practice*; Springer: New York, 2010; Chapter 6, pp 251−289.
(29) Berenschot, E. J. W.; Jansen, H. V.; Tas, N. R. Fabrication of 3D fractal structures using nanoscale anisotropic etching of single crystalline silicon. *J. Micromech. Microeng.* **2013**, *23*, 055024−055033.
(30) Weisse, J. M.; Lee, C. H.; Kim, D. R.; Cai, L.; Rao, P. M.; Zheng, X. Electroassisted Transfer of Vertical Silicon Wire Arrays Using a Sacrificial Porous Silicon Layer. *Nano Lett.* **2013**, *13*, 4362−4368.
(31) Mallory, G. O. In *Electroless Plating: Fundamentals and Applications*; John Wiley & Sons: Hoboken, NJ, 1990; Chapter 1, pp 1−47.
(32) Schlesinger, M. In *Modern Electroplating*; John Wiley & Sons: Hoboken, NJ, 2011; Chapter 18, pp 447−458.
(33) Schweitzer, G.; Pesterfield, L. In *The Aqueous Chemistry of the Elements*; Oxford University Press: New York, 2009; Chapter 8, pp 173−199.
(34) Buhler, J.; Steiner, F.-P.; Baltes, H. Silicon dioxide sacrificial layer etching in surface micromachining. *J. Micromech. Microeng* **1997**, *7*, R1−R13.
(35) Hall, D. S.; Lockwood, D. J.; Bock, C.; MacDougall, B. R. Nickel hydroxides and related materials: a review of their structures, synthesis and properties. *Proc. R. Soc. London, Ser. A* **2015**, *471*, 20140792−20140792.
(36) Palmer, D. A.; Bénézeth, P.; Wesolowski, D. J. Solubility of Nickel Oxide and Hydroxide in Water. In *14th International Conference on the Properties of Water and Steam in Kyoto*, 2004; pp 264−269.
(37) Gayer, K. H.; Garrett, A. B. The Equilibria of Nickel Hydroxide, Ni(OH), in Solutions of Hydrochloric Acid and Sodium Hydroxide. *J. Am. Chem. Soc.* **1949**, *71* (71), 2973−2975.
(38) List of Controlled Substances and Precursor Chemicals − Stanford Environmental Health and Safety. Available at: https://ehs.stanford.edu/reference/list-controlled-substances-and-precursor-chemicals.
(39) Furukawa, S.; Mehregany, M. Electroless plating of nickel on silicon for fabrication of high-aspect-ratio microstructures. *Sens. Actuators, A* **1996**, *56*, 261−266.
(40) Takano, N.; Hosoda, N.; Yamada, T.; Osaka, T. Mechanism of the Chemical Deposition of Nickel on Silicon Wafers in Aqueous Solution. *J. Electrochem. Soc.* **1999**, *146*, 1407−1411.
(41) Sudagar, J.; Lian, J.; Sha, W. Electroless nickel, alloy, composite and nano coatings - A critical review. *J. Alloys Compd.* **2013**, *571*, 183−204.
(42) Hsu, H. F.; Tsai, C. L.; Lee, C. W.; Wu, H. Y. Mechanism of immersion deposition of Ni−P films on Si(100) in an aqueous alkaline solution containing sodium hypophosphite. *Thin Solid Films* **2009**, *517*, 4786−4791.
(43) Pomogailo, A. D.; Dzhardimalieva, G. I. In *Nanostructured Materials Preparation via Condensation Ways*; Springer Netherlands: Rotterdam, Netherlands; 2014; Chapter 2, pp 13−89.
(44) Smith, R.; Martell, A. Critically Selected Stability Constants of Metal Complexes Database, National Institute of Standards and Technology, 2004.
(45) Loto, C. A. Electroless Nickel Plating − A Review. *Silicon* **2016**, *8*, 177−186.
(46) Lo, Y. L.; Hwang, B. J. Decomposition of NaBH4 in an Electroless Nickel Bath. *Ind. Eng. Chem. Res.* **1994**, *33*, 56−61.
(47) Sone, M.; Mark, T.-F.; Uchiyam, H. In *Advanced Topics on Crystal Growth*; InTech: 2013; Chapter 11, pp 335−372.
(48) Park, G. D.; Cho, J. S.; Kang, Y. C. Sodium-ion storage properties of nickel sulfide hollow nanospheres/reduced graphene oxide composite powders prepared by a spray drying process and the nanoscale Kirkendall effect. *Nanoscale* **2015**, *7*, 16781−16788.
(49) Mansour, A. N. Characterization of NiO by XPS. *Surf. Sci. Spectra* **1994**, *3*, 231−238.
(50) Logofatu, C.; Negrila, C. C.; Ghita, R. V.; Ungureanu, F.; Cotirlan, C.; Manea, C. G. A. S.; Lazarescu, M. F. In *Cyrstalline Silicon - Properties and Uses*; InTech: 2011; Chapter 2, pp 23−41.
(51) Khassin, A. A.; Yurieva, T. M.; Demeshkina, M. P.; Kustova, G. N.; Itenberg, I. S.; Kaichev, V. V.; Plyasova, L. M.; Anufrienko, V. F.; Molina, I. Y.; Larina, T. V.; Baronskaya, N. A.; Parmon, V. N. Characterization of the nickel-amesite-chlorite-vermiculite system. Part I. Silicon binding in Ni−Mg−Al phylloaluminosilicates. *Phys. Chem. Chem. Phys.* **2003**, *5*, 4025−4031.
(52) Li, H.; Ye, T.; Shi, L.; Xie, C. Fabrication of ultra-high aspect ratio (>160:1) silicon nanostructures by using Au metal assisted chemical etching. *J. Micromech. Microeng.* **2017**, *27*, 124002.

DOI: 10.1021/acsami.8b06002
ACS Appl. Mater. Interfaces 2018, 10, 22834−22840